Journal of Atmospheric and Solar-Terrestrial Physics 71 (2009) 365–372

Contents lists available at ScienceDirect

Journal of Atmospheric and Solar-Terrestrial Physics

journal homepage: www.elsevier.com/locate/jastp

Comparison of polar mesospheric cloud measurements from the Cloud Imaging and Particle Size experiment and the solar backscatter ultraviolet instrument in 2007

Susanne Benze [a,*], Cora E. Randall [a], Matthew T. DeLand [b], Gary E. Thomas [c], David W. Rusch [c], Scott M. Bailey [d], James M. Russell III [e], William McClintock [c], Aimee W. Merkel [c], Chris Jeppesen [c]

[a] Laboratory for Atmospheric and Space Physics & Department of Atmospheric and Oceanic Sciences, University of Colorado at Boulder, 392 UCB, Boulder, CO 80309-0392, USA
[b] Science Systems and Applications Inc. (SSAI), Greenbelt, MD, USA
[c] Laboratory for Atmospheric and Space Physics, 1234 Innovation Drive, Boulder, CO 80303, USA
[d] Bradley Department of Electrical and Computer Engineering, Virginia Polytechnical and State University, Blacksburg, VA 24061, USA
[e] Center for Atmospheric Sciences, Hampton University, Hampton, VA, USA

ARTICLE INFO

Article history:
Accepted 22 July 2008
Available online 5 August 2008

Keywords:
Polar Mesospheric Cloud
PMC
SBUV
AIM
Validation
Noctilucent cloud

ABSTRACT

We compare measurements from the Aeronomy of Ice in the Mesosphere (AIM) Cloud Imaging and Particle Size (CIPS) experiment to the NOAA-17 solar backscatter ultraviolet (SBUV/2) instrument during the 2007 Northern Hemisphere polar mesospheric cloud (PMC) season. Daily average Rayleigh scattering albedos determined from identical footprints from the CIPS nadir camera and SBUV/2 agree to better than ~5% throughout the season. Average PMC brightness values derived from the two instruments agree to within $\pm 10\%$. PMC occurrence frequencies are on average ~5% to nearly a factor of two higher in CIPS, depending on latitude. Agreement is best at high latitudes where clouds are brighter and more frequent. The comparisons indicate that AIM CIPS data are valid for scientific analyses. They also show that CIPS measurements can be linked to the long time series of SBUV/2 data to investigate long-term variability in PMCs.

1. Introduction

Polar mesospheric clouds (PMCs) are very thin ice clouds forming in the summer mesopause region. They are generally referred to as noctilucent clouds (NLC) when viewed or measured from the ground. It has been suggested that they are related to climate change in the upper atmosphere (Thomas, 1996a; Thomas et al., 1991). As tracers of upper atmosphere water vapor (H_2O) and temperature, PMCs can be used to understand the dynamics of the upper mesosphere. Thomas et al. (1989) first suggested that increases in mesospheric H_2O resulting from increased methane would lead to brighter PMCs. DeLand et al. (2003) suggested that this might lead to an earlier (later) first appearance of NLCs during evening (morning) twilight, whereas Thomas (1996b) proposed that it could cause PMCs to shift to lower latitudes, which was supported by Taylor et al. (2002). AIM is the first satellite mission specifically dedicated to measuring PMCs. The mission is designed to elucidate the connections between PMCs and mesospheric H_2O, temperature, and dynamics, with an overall goal of understanding how PMCs form and why they vary (Russell et al., 2008). AIM was recently extended for another 3 years, making it a 5-year mission. This enables investigation of interannual observations, solar cycle effects, hemispheric differences, and teleconnections among other things.

The Cloud Imaging and Particle Size (CIPS) experiment is a panoramic imager with a field of view of 120° (along track) by 80° (cross-track) or about 2000×1000 km; it is described in more detail by Russell et al. (2008) and McClintock et al. (2008). CIPS has an unprecedented spatial resolution of ~2 km in the nadir. In order to derive PMC morphology and cloud particle size, CIPS measures scattered sunlight with a 15 nm passband centered at 265 nm. The observed signals include Rayleigh scattering by atmospheric gases as well as scattering by the PMCs themselves. The Rayleigh scattering signal must therefore be separated from

* Corresponding author. Tel.: +1 303 492 3260; fax: +1 303 492 6946.
E-mail addresses: susanne.benze@lasp.colorado.edu (S. Benze), randall@lasp.colorado.edu (C.E. Randall), matthew_deland@ssaihq.com (M.T. DeLand), gary.thomas@lasp.colorado.edu (G.E. Thomas), Dave.Rusch@lasp.colorado.edu (D.W. Rusch), baileys@vt.edu (S.M. Bailey), James.Russell@hamptonu.edu (J.M. Russell III), William.McClintock@lasp.colorado.edu (W. McClintock), aimee.merkel@lasp.colorado.edu (A.W. Merkel), jeppesen@lasp.colorado.edu (C. Jeppesen).

1364-6826/$ - see front matter © 2008 Elsevier Ltd. All rights reserved.
doi:10.1016/j.jastp.2008.07.014

the observed signal to infer PMCs. The method by which this is accomplished is described in Section 2. Radiation at 265 nm penetrates to an altitude of about 50 km; the atmospheric Rayleigh scattering signal is thus modulated by upper stratospheric and mesospheric ozone absorption in the Hartley–Huggins band as the radiation propagates along the incident and scattered light paths. Chandran et al. (2008) use ice signatures to derive information regarding gravity waves; and Merkel et al. (2008) analyze the clouds detected by CIPS to derive information on planetary wave activity in the mesosphere. Rusch et al. (2008) describe features in the CIPS cloud data that are likely caused by various dynamical phenomena.

The primary goal of this paper is to show that the AIM CIPS data are of high quality, and valid for the types of scientific analyses described above. This is accomplished by comparing CIPS measurements to concurrent measurements from the NOAA-17 solar backscatter ultraviolet (SBUV/2) instrument (e.g., Frederick et al., 1986; Heath et al., 1975). The SBUV/2 instruments have a long history of PMC measurements, spanning several decades. Therefore, these comparisons also show that the CIPS measurements can be linked to the long time series of SBUV data to investigate long-term variability in PMCs. With its unprecedented high resolution, CIPS data can be used to account for possible biases in the SBUV data set that might result from its lower-resolution sampling, ensuring that long-term trends are interpreted correctly. Because of the coincident information on such atmospheric parameters as mesospheric temperature and water vapor measured by the Solar Occultation For Ice Experiment (SOFIE) (Russell et al., 2008) and the Sounding of the Atmosphere using Broadband Emission Radiometry (SABER) (Russell et al., 1999), we can ultimately address the question of the origin of long-term variability, one of the scientific objectives of AIM. Quantitative comparisons with global models will be possible, validating the physical mechanism of cloud formation and the origin of long-term variability in PMC properties.

The SBUV/2 instruments are nadir-pointed, and measure backscattered radiation at 12 different wavelengths ranging from 252 to 340 nm. Unlike CIPS, the SBUV/2 instruments are not imagers; rather, the field of view consists of a single footprint of $11.3^\circ \times 11.3^\circ$, or about 150 km $\times$ 150 km at the PMC altitude. The SBUV/2 instruments were originally designed to measure ozone, but have been used to measure PMCs (Thomas et al., 1991; DeLand et al., 2003, 2006, 2007). For the comparisons shown here, the CIPS data were analyzed in the same manner as the SBUV/2 data, as described in Section 2. We use level 1a CIPS data, version 3. We restrict the comparisons here to the NOAA-17 SBUV/2 data, since the local times of measurements from this satellite more closely match the CIPS local times than measurements from other SBUV/2 instruments. The SBUV/2 data correspond to version 3. SBUV data have been validated extensively with instruments measuring profile and column ozone as well as PMCs. The integrated ozone columns measured by SBUV and the Stratospheric Aerosol and Gas Experiment between October 1984 and June 1990 agree to within $\pm 2.3\%$ at all latitudes (McPeters et al., 1994). Thomas et al. (1991) showed that SBUV correlates well with contemporaneous Solar Mesosphere Explorer (SME) PMC data: the seasonal and latitudinal variations of PMCs are similar, and correcting for different sensitivities of the instruments, the general magnitude of the SBUV residuals is consistent with that expected from SME data. DeLand et al. (2003) extended this comparison to SBUV/2 and found that NOAA-9 SBUV/2, Nimbus-7 SBUV and SME results for the 1985 and 1986 seasons were very similar in magnitude and temporal structure when different sensitivities and scattering angles were accounted for. Using a more recent PMC detection algorithm, DeLand et al. (2007) showed even better agreement between various SBUV/2 instruments in both hemispheres.

2. Cloud detection algorithm

Both the SBUV/2 and CIPS instruments measure radiance backscattered by the atmosphere and clouds. The albedo (unit of sr^{-1}) is obtained by dividing the radiance by the solar irradiance. This section describes the method by which we separate the contributions to the albedo from "background" Rayleigh scattering and PMC scattering. As described by Bailey et al. (2008), one approach to separating Rayleigh scattering from cloud scattering takes advantage of the fact that CIPS is capable of measuring the scattering phase function. That is, CIPS takes multiple exposures of the same region of the atmosphere at different scattering angles. Since scattering by the relatively large particles in clouds is described by a different phase function than Rayleigh scattering, this principle can be utilized to separate the background Rayleigh scattering from the PMCs. This approach is not possible with the SBUV/2 instrument, since it does not measure the same region of space at multiple scattering angles. Thus, the Rayleigh background removal technique used for the CIPS/SBUV comparisons is based on a simplification of the method described by DeLand et al. (2003), which is applied to both the CIPS and SBUV/2 data.

In the SBUV/2 data, PMCs appear as spectrally dependent enhancements of the background (Rayleigh scattering) signal. Since the CIPS instrument does not have multi-wavelength data, the standard SBUV/2 cloud detection algorithm, which takes advantage of the spectral dependence, cannot be applied directly to the CIPS data. Therefore, the standard algorithm was modified to a single-wavelength approach, and the modified algorithm was applied to both the SBUV/2 and CIPS data. Here we describe the standard SBUV/2 algorithm, then compare results from it to the modified algorithm.

In the standard SBUV/2 analysis, the background albedo is defined as a fourth-order polynomial fit to the observed albedo as a function of solar zenith angle (SZA), including all measurements on a given day. The fit is calculated for data acquired at each of five UV wavelengths (DeLand et al., 2003). As an example, the top left plot of Fig. 1 shows the SBUV/2 albedo as a function of SZA at 273 nm on 20 July 2007. For a nadir instrument like SBUV/2 the SZA can be converted to the solar scattering angle (SCA): $\mathrm{SCA} = 180^\circ - \mathrm{SZA}$. Therefore, the background albedo decreases (increases) with increasing SZA (SCA) between 0° and 90° SZA (90° and 180° SCA), as expected for Rayleigh scattering. The difference between the albedo values and the background fit is defined as the albedo residual or, for clouds, the PMC brightness for each wavelength. The residuals for this example are shown in the bottom left plot of Fig. 1.

In order to identify clouds in the SBUV/2 data, the standard algorithm applies several wavelength-dependent tests to the albedo residuals, as described by DeLand et al. (2003) and updated by DeLand et al. (2007). The first test requires that the albedo residuals at the three shortest wavelengths are positive. The second test is based on the fact that for the small particle sizes expected of PMCs, the PMC scattering will be stronger at shorter wavelengths; this imposes the requirement that the slope of a linear regression fit to the five residuals be negative. Other tests require the 252-nm albedo residual to exceed the 273-nm albedo residual and the albedo to exceed a noise threshold. The last test requires the residual to exceed the smaller of either an absolute ($7 \times 10^{-6}\,sr^{-1}$) or relative (1.05 times the average background) threshold. The last test will be referred to here as the absolute/relative threshold test. All these tests are run five times iteratively, with successive iterations including only those points that were

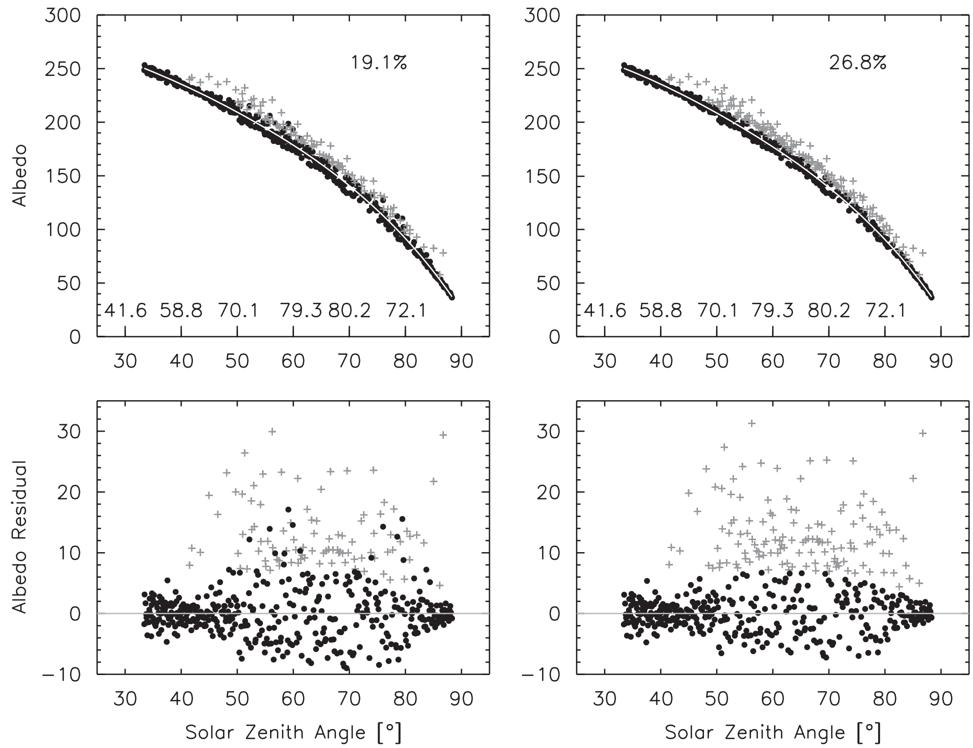

Fig. 1. Comparison of the albedo (top) and albedo residual (bottom) derived from the standard SBUV/2 cloud detection algorithm ("all-λ", left) and the modified, single-wavelength algorithm ("one-λ", right) applied to NOAA-17 SBUV/2 data from 20 July 2007. The one-λ algorithm uses the SBUV/2 273-nm channel. Albedo and albedo residual units on all plots are $10^{-6}\,sr^{-1}$. Black, closed circles denote non-cloud points; gray, plus symbols represent cloud detections. Labels just above the horizontal axis in the top panels denote measurement latitudes. The white line in the top panels indicates the fourth-order polynomial fit to the background.

identified as "background". That is, points that pass the tests on any iteration are identified as clouds, and not included in successive iterations. After five iterations, any point not already identified as a cloud is identified as background. The left panels of Fig. 1 show SBUV/2 cloud identifications for 20 July 2007 that were based on this multi-wavelength identification procedure.

For application to CIPS data, which measures at only one wavelength, the algorithm was modified to require only that the residuals for clouds be positive and pass the absolute/relative threshold test. In the following, the original cloud detection algorithm described by DeLand et al. (2003, 2007) will be referred to as the "all-λ" algorithm, whereas the modified algorithm will be referred to as the "one-λ" algorithm. To estimate the error introduced by removing the spectral information from the cloud identification algorithm, the one-λ algorithm was applied to SBUV/2 data and the results compared with those obtained using the all-λ algorithm. The SBUV/2 wavelength used was 273 nm, which is the SBUV/2 channel that is closest to the center of the CIPS bandpass at 265 nm. The SBUV spectral response at 273.61 nm is quite narrow and essentially monochromatic (Fleig et al., 1990). We have performed a detailed examination of the effects of the CIPS bandpass function, convolved with the back-scattered solar radiance spectrum and the smooth spectral dependence of PMC, to find the correction needed to relate the CIPS albedo to the equivalent monochromatic albedo. We find that at 273 nm, the correction factor is fortuitously unity. So for comparison of SBUV/2 at 273 nm and CIPS at 165 nm, no correction was necessary. Further, the 273-nm channel has a signal-to-noise ratio that is ~4–5 times higher than the 252-nm channel.

Fig. 1 illustrates the comparisons between the all-λ and one-λ algorithms with a single day of data on 20 July 2007. As noted above, the left panels display clouds identified with the all-λ algorithm; the right panels display clouds identified with the one-

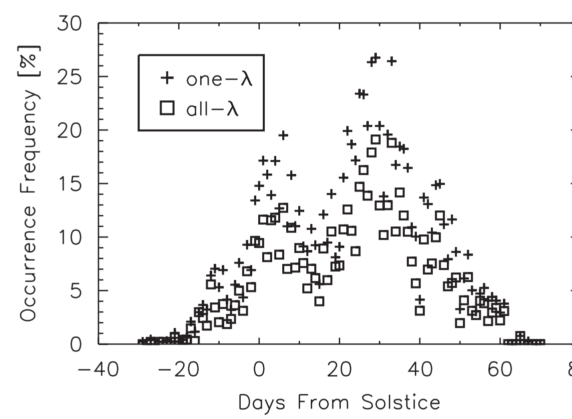

Fig. 2. Daily occurrence frequencies (number of clouds divided by the total number of measurements on any given day, in %) from NOAA-17 SBUV/2 data calculated using the all-λ (squares) and 273-nm one-λ (plus symbols) algorithms. Measurement latitudes are restricted to 50–90°N.

λ algorithm. The occurrence frequency, which is defined as the ratio of the number of cloud observations to the number of measurements per day, was 19.1% with the all-λ algorithm and 26.8% with the one-λ algorithm. The one-λ cloud detection algorithm results in a higher occurrence frequency because fewer tests are required, making it less stringent. The bottom panels of Fig. 1 clearly differentiate between the clouds and background, showing that there is no systematic pattern with respect to SZA. Most of the clouds detected by the one-λ algorithm that are not detected by the all-λ algorithm have brightness values that are close to the background (non-cloud) level, but not all. In general, however, the one-λ algorithm gives results that are close to the all-λ algorithm. This is represented statistically in Fig. 2, which shows the occurrence frequency vs. day of year for the one-λ and

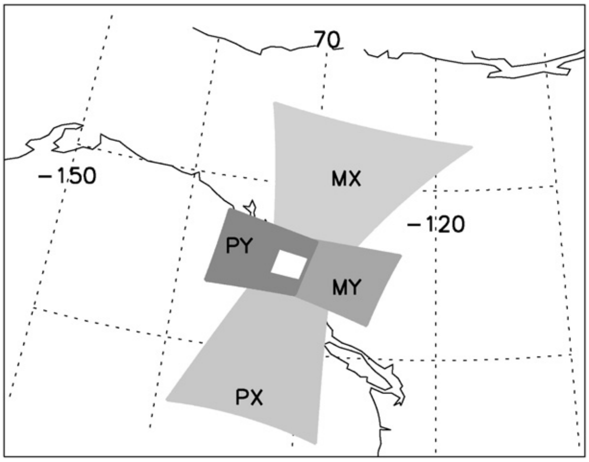

Fig. 3. Viewing geometry for the CIPS cameras, with the SBUV/2 field of view (white) superimposed.

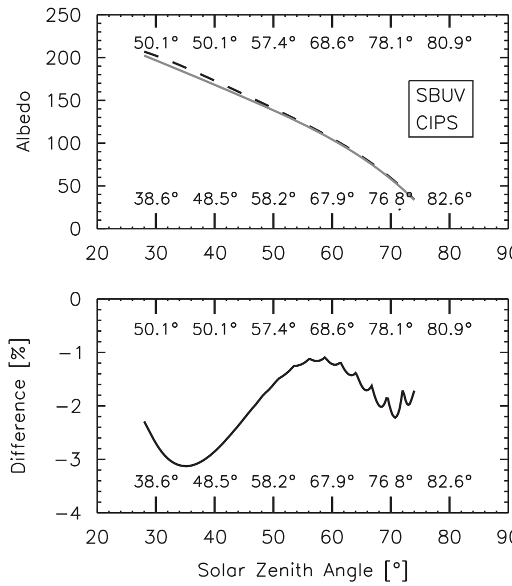

Fig. 4. Fourth-order polynomial fits to the background albedo (top) for CIPS (gray solid) and NOAA-17 SBUV/2 (black dashed) at 273 nm and the difference between the fits (bottom) for overlapping SZA ranges on 30 August 2007. Albedo units are $10^{-6}\,\mathrm{sr}^{-1}$. Labels above (below) the bottom (top) horizontal axes give measurement latitudes for CIPS (SBUV).

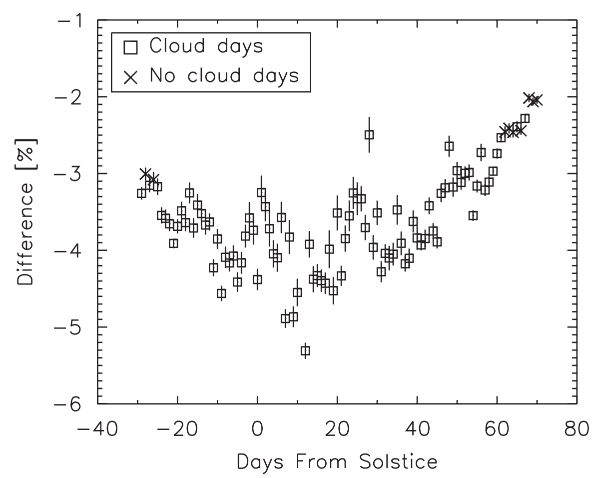

Fig. 5. Average difference between the polynomial fits to the background for CIPS and SBUV/2 at 273 nm vs. day of year for the NH in 2007. "Error" bars represent 1-σ standard deviation of the mean difference on each day.

all-λ algorithms, for all SBUV/2 data over the entire Northern Hemisphere (NH) season in 2007. The one-λ algorithm reproduces the temporal variation in cloud frequencies very well throughout the season, but with a high bias. The average frequency over the whole season is 11% for the one-λ case and 8% for the all-λ case. Note that results are similar if only the brightest clouds are included in the analysis. We conclude from this analysis that the one-λ algorithm is suitable for comparing CIPS and SBUV/2 data to evaluate the CIPS data, although frequencies might be overestimated for both instruments.

To further ensure that the data sets are analyzed in a consistent manner, the CIPS measurements were binned into a footprint that matches the SBUV/2 footprint of $\sim$150 km $\times$ 150 km at cloud altitude. Thus a single SBUV/2 measurement corresponds to the average of more than 5000 CIPS pixels. This results in an improvement in signal-to-noise ratio from 5.2 in a single-pixel measurement of the background Earth albedo (Russell et al., 2008) to more than 350 for the binned data. Fig. 3 illustrates the viewing geometries of CIPS and SBUV/2; all CIPS pixels within the SBUV/2 footprint indicated in white were binned together for the comparisons described below. Results are shown below for the CIPS PY camera (see Fig. 3), but they are essentially identical for the MY camera.

3. Results and discussion

An accurate retrieval of the Rayleigh background is fundamental for proper cloud detections. Fig. 4 compares the background polynomial fits to CIPS and SBUV/2 data for 30 August 2007, a day when no clouds were detected. The top plot shows the albedo vs. SZA, with CIPS in solid gray and SBUV/2 in dashed black. The bottom plot shows the percent difference between the two instruments in the overlapping SZA ranges. For this day the CIPS background is on an average about 2% lower than the SBUV/2 background, representing one of the more favorable comparisons in the data set. Differences are largest at low solar zenith angles, which is likely explained by the fact that the measurement latitudes are significantly different at these SZA values. Fig. 5 gives an overview of the background differences vs. day of year in 2007. The differences here are calculated as the average of the differences vs. solar zenith angle on each day (e.g., the average of the bottom curves in Fig. 4, averaged over the entire season). CIPS is systematically lower than SBUV/2, but differences are smaller than 5%, with the exception of one day in July.

There is an interesting time dependence in the background differences. At the beginning and end of the time period, when few or no clouds are present, the agreement is better than in the middle of the season. This could suggest that clouds lead to larger background differences, but this suggestion is contradicted by the behavior of the differences in the middle of the season. That is, temporal variations during the cloud season appear to reflect some of the same variations seen in the cloud frequencies in Fig. 2. Peaks in frequency occur near 0 and 30 days since solstice; this corresponds approximately to decreases, not increases, in the background differences shown in Fig. 5. One explanation for this apparent contradiction pertains to the relative brightness of the clouds that are present. Correct calculation of the background requires identification of clouds above the background variability, which is caused primarily by fluctuations in ozone densities (e.g., DeLand et al., 2007) and measurement error. At the beginning and end of the season, clouds are less frequent and on average

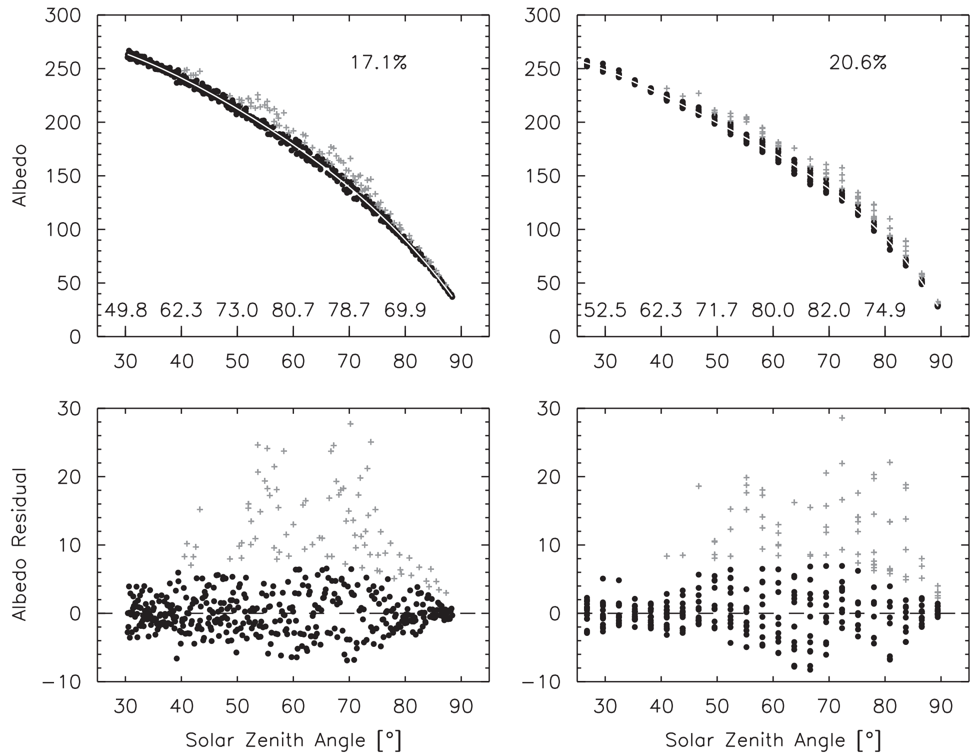

Fig. 6. Left: Similar to the right panels in Fig. 1, but for NOAA-17 SBUV/2 data at 273 nm on 22 June 2007; gray plus symbols denote PMCs. Right: Same as left, but for CIPS data on 22 June 2007. Albedo and albedo residual units are $10^{-6}\,sr^{-1}$.

relatively dim, so even incorrect identification does not lead to significant errors in the background calculation. In the middle of the season, however, incorrect identification of relatively dim clouds can lead to significant errors in the background because the clouds are so much more numerous. The larger or relatively brighter clouds are more easily distinguished from the background variability, and thus are not expected to lead to significant errors. As shown below (see Fig. 9), near days 0 and 30 when the cloud frequencies increased, the average cloud brightness also increased. Thus, we speculate that the background calculations should improve near days 0 and 30 since the brighter clouds present at these times are more easily identified, and therefore do not contaminate the background calculation.

Fig. 6 shows cloud detections for 22 June 2007 from both SBUV/2 (left) and CIPS (right). The top (bottom) plots show albedo (albedo residual) vs. SZA, with clouds denoted as gray plus symbols. Both the albedo and albedo residual values compare well with each other, with a minimum near 60–65° SZA and relative maxima near 55° and 70° SZA. The CIPS occurrence frequency of 20.6% is higher than the 17.1% occurrence frequency of SBUV/2; this is discussed more below. Interestingly, the background (non-cloud) residuals here are very similar in the SBUV/2 and CIPS data. Since the binned CIPS data have such low noise (<0.5%), the variability seen here is very likely real, and caused by ozone fluctuations.

Fig. 7 shows a qualitative comparison of the latitude dependence of CIPS and SBUV/2 cloud frequencies throughout the season. Both instruments show an asymmetric pattern, with cloud frequencies reaching maximum latitudinal extent near the summer solstice before gradually diminishing in extent over the next 60 days. Both instruments also show a marked decrease in frequency about 10–20 days after solstice that extends across all latitudes. These kinds of patterns have also been noted in other satellite observations of PMCs (e.g., Bailey et al., 2005). Noteworthy is that, consistent with the single-day result in Fig. 6, the

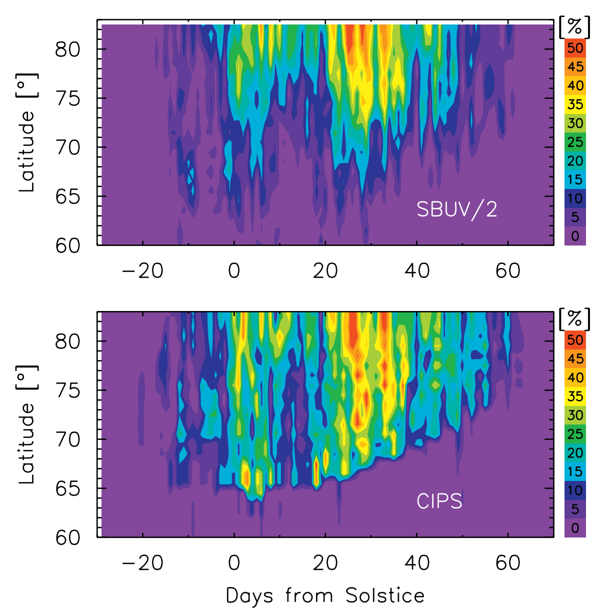

Fig. 7. Daily PMC cloud occurrence frequency from NOAA-17 SBUV/2 data at 273 nm (top) and CIPS (bottom) in the NH in 2007. Occurrence frequencies (%) are calculated as the number of measurements identified as clouds relative to the total number of measurements in 2° latitude bins.

CIPS frequencies are generally higher than the SBUV/2 frequencies throughout the season and at all latitudes, as quantified next.

Figs. 8 and 9 compare the occurrence frequency and PMC brightness for three different latitude ranges (60–70°N, 70–80°N, and 80–83°N) for CIPS (red) and SBUV/2 (blue). The third latitude range extends only to 83°N because this is the highest latitude either instrument samples. Overall both the frequency and brightness of the two instruments compare very well to each other, but with some latitude dependence. The CIPS frequency is higher than the SBUV/2 frequency, as already noted, but the morphology is similar. Averaged over the season, the frequencies for CIPS (SBUV) are 8% (4%), 19% (15%), and 23% (22%) for the latitude bands from 60° to 70°N, 70° to 80°N, and 80° to 83°N, respectively. That frequencies compare better at higher latitudes might be due in part to the fact that measurement locations for the two instruments are closer together at the high latitudes. It is probably also related to the fact that cloud brightness increases with increasing latitude, as shown in Fig. 9. Cloud detections are more robust for the brighter clouds because they are easier to distinguish from the background (DeLand et al., 2007). The average cloud brightness values for CIPS (SBUV/2) are 6.7×10^{-6} sr^{-1} ($7.4\times10^{-6}\,sr^{-1}$), $10.3\times10^{-6}\,sr^{-1}$ ($10.0\times10^{-6}\,sr^{-1}$), and $12.2\times10^{-6}\,sr^{-1}$ ($11.2\times10^{-6}\,sr^{-1}$) for the respective latitude bands. Thus on average the brightness values derived from CIPS and SBUV/2 agree to within 10%. We speculate that the higher CIPS frequencies at the lower latitudes arise because low-intensity clouds are more likely to be detected as noise on the background in the SBUV data, but actual clouds in the CIPS data. This is also consistent with the background comparisons shown in Fig. 5. If low-intensity clouds are identified incorrectly as background in the SBUV/2 data, they will raise the background level, resulting in a background in CIPS that is lower than in SBUV/2.

The results shown above include all of the available measurements from the two instruments, regardless of location and local time. To examine the possibility that these results were biased because of different measurement sampling, comparisons were repeated using only those measurements from both instruments that were within 100 km and 1 h in local time. Although geophysical variations can take place on these scales, this was considered a reasonable trade-off between minimizing differences

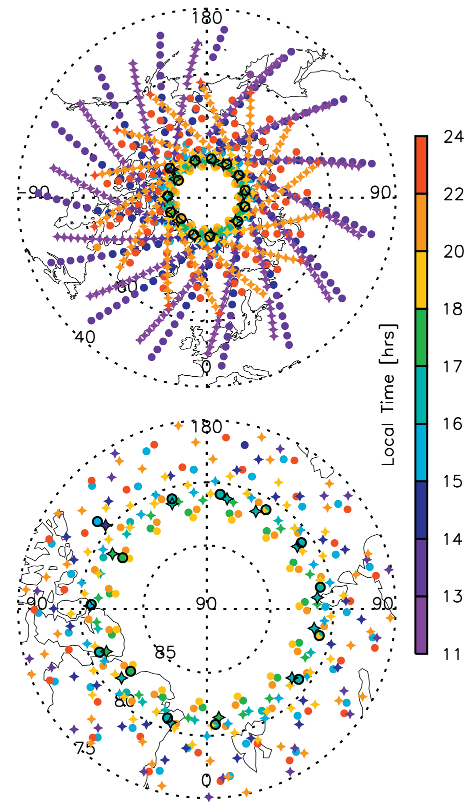

Fig. 10. Coincidences (framed symbols) overlaid on all measurements from CIPS (circles) and NOAA-17 SBUV/2 (stars) on 27 June 2007, for all latitudes (top) and only high latitudes (bottom). Symbols are color coded by their local time.

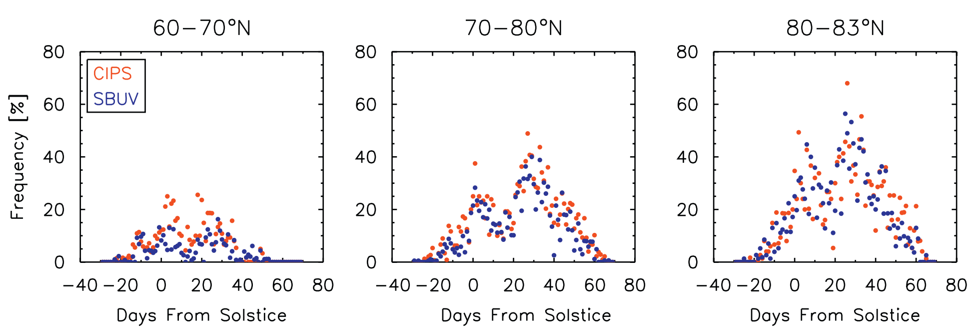

Fig. 8. CIPS (red) and SBUV/2 (blue) PMC occurrence frequency vs. day of year for three different latitude ranges. Here the occurrence frequencies (in %) are calculated as the number of measurements identified as clouds relative to the total number of measurements in the latitude bins specified at the top of each panel.

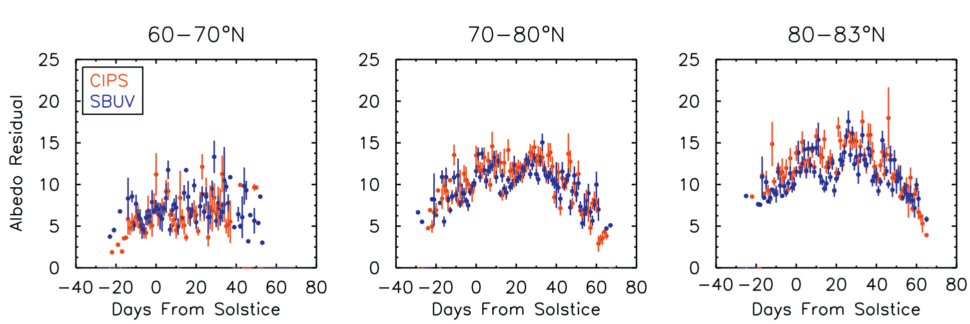

Fig. 9. Same as Fig. 8, but for daily average albedo residuals pertaining to cloud detections in the specified latitude bins (observed albedo minus the polynomial fit to the background, so this represents the cloud brightness). The albedo residuals have units of $10^{-6}\,sr^{-1}$. "Error" bars represent 1-σ standard deviation of the mean PMC albedo residual on each day.

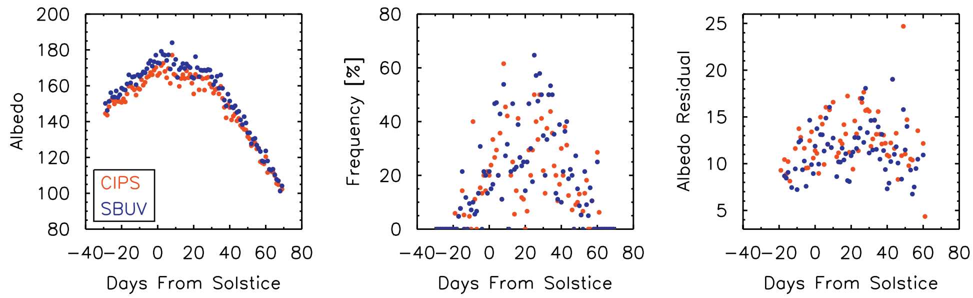

Fig. 11. Daily average albedo (left, $10^{-6}\,sr^{-1}$), daily occurrence frequency (middle), and daily average PMC brightness (right, $10^{-6}\,sr^{-1}$), for the NH 2007 season from CIPS (red) and NOAA-17 SBUV/2 at 273 nm (blue). Albedos are calculated as the average of the albedos at coincident measurement locations on each day. Albedo residuals are calculated similarly; the background subtracted from the albedo to yield the residual was determined from the full set of measurements, not just coincidences. Occurrence frequencies (%) refer to the number of coincident measurements identified as clouds relative to the total number of coincident measurements on each day.

in the observed atmospheric region and obtaining significant statistics. Fig. 10 shows the SBUV/2 and CIPS nadir locations on 27 June 2007 (symbols do not correspond to actual footprint size). The framed symbols depict the coincidences. All symbols are color coded for their local time. The top plot shows the measurement locations for the whole latitude range of the measurements for that day (40–90°), whereas the bottom plot is restricted 75–90° in order to better display the coincidences. Over the entire season there were 1372 coincidences between CIPS and SBUV/2, or about 16 coincidences per day (ranging from 9 to 23). Most coincidences were between 78° and 82°N because local time changes rapidly as the satellites cross the polar cap and go from the day side into the night side of the Earth. Note that the number of coincidences is limited by the nadir-viewing constraint we have placed on the current analysis; many more coincidences will be available for future comparisons using all CIPS viewing angles.

Fig. 11 shows the results of the coincidence comparisons. The full cloud detection analysis was not repeated because the lack of data compromises the background simulation. Rather, for Fig. 11 the daily average quantities were simply re-calculated using only the coincident data points, but utilizing the background albedo derived with the full data set. To the extent that different measurement sampling affects the background determination, these results are similar to the non-coincident results shown above; they should, however, be less affected by PMC variability. Fig. 11 shows the comparisons for daily average albedo (cloud+background), frequency, and daily average albedo residual (albedo minus background) for all coincident measurements. As expected from the comparisons discussed above, all three panels show excellent agreement. The average albedo over the season was $149\times10^{-6}\,sr^{-1}$ ($154\times10^{-6}\,sr^{-1}$) for CIPS (SBUV/2), a difference of only 3%. The average daily cloud frequency over the season was 24% (27%), and the average cloud brightness over the season was 13% (12%) for CIPS (SBUV/2). These results are similar to the results of the non-coincidence analysis, suggesting that sampling issues are not a significant factor in the comparisons.

4. Conclusions

We have described comparisons between AIM CIPS and SBUV/2 Rayleigh scattering and PMC scattering measurements. A single cloud detection algorithm was applied to data from both instruments, and the high spatial resolution CIPS data were binned to match the SBUV/2 footprint. The CIPS data were thus restricted to the nadir, while SBUV/2 data were restricted to the 273-nm channel. The cloud detection algorithm was based on the standard SBUV/2 cloud detection algorithm, but ignored all spectral information.

The comparisons show that CIPS and SBUV/2 measurements are in excellent agreement. The daily average Rayleigh scattering backgrounds determined from the two instruments agree to better than ~5% throughout the season. Average CIPS PMC brightness values are within 10% of the SBUV values. CIPS daily PMC occurrence frequencies are generally higher than those from SBUV/2, with differences decreasing at high latitudes where the clouds are brighter and more frequent. From 60° to 70°N the average frequencies differed by a factor of two, but this decreased to less than 5% from 80° to 83°N. We tentatively attribute the frequency differences to the fact that binning the CIPS data into the SBUV footprint significantly improves the signal-to-noise, making it more likely that dim clouds are properly identified as such in the CIPS data. We note, however, that the single-wavelength algorithm applied here does not take advantage of the full capabilities of the SBUV/2 data, since it ignores spectral information.

We conclude from the above comparisons that the CIPS nadir data are valid for scientific analysis. It should be noted that only a tiny fraction of the available CIPS data has actually been used. Nadir data within the SBUV/2 footprints from the PY camera represent less than 0.001% of the CIPS data. In the analysis presented above, the high spatial resolution of the CIPS data as well as the scattering angle dependence has been lost. Extended algorithms are necessary to take advantage of these unique CIPS features, such as described by Bailey et al. (2008). Data produced with this type of extended algorithm was used in the analyses of Chandran et al. (2008), Rusch et al. (2008) and Merkel et al. (2008). Although the current paper does not provide direct validation of the data used in those papers, the above results do indicate that the cameras are performing as expected. Further, the results in the nadir pixels analyzed here are consistent with the broader results described in those papers. An example is shown here in Fig. 12. This figure portrays the average NH PMC occurrence frequency as a function of day and longitude during the 2007 season, for latitudes from 75° to 85°N. SBUV/2 results are shown in the top panel; CIPS results (bottom) include only the data binned into the SBUV/2 footprint. Not only do the results agree with each other, as expected from the comparisons shown above, but they also agree with the more comprehensive analysis described by Merkel et al. (2008). That paper uses all of the CIPS data to explore the occurrence of planetary wave activity in the CIPS data, which is seen clearly in both the nadir CIPS and SBUV/2 data here. The comparisons shown here thus serve not only to validate the nadir CIPS data, but also to lend credibility to the off-nadir measurements as well. Finally, that CIPS data binned to match the SBUV/2 spatial resolution compare so well to SBUV/2

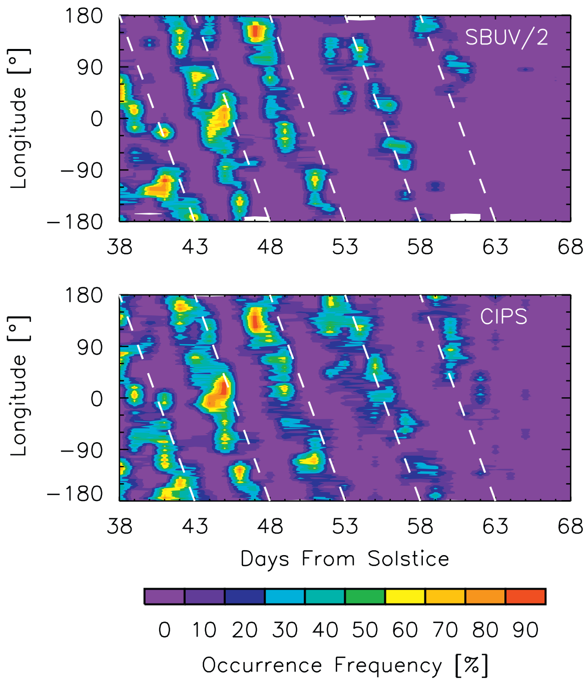

Fig. 12. Daily occurrence frequency from 75° to 85°N plotted vs. longitude for SBUV/2 at 273 nm (top) and CIPS (bottom) in the NH in 2007. Frequencies represent a running average over 20° in longitude. White, dashed lines are drawn only for guidance; they indicate the tilt that would be expected for a 5-day wave. See Merkel et al. (2008) for discussion of wave activity inferred from CIPS data.

data supports the goal of linking the long time series of SBUV/2 data to the CIPS data in order to investigate long-term variability in PMCs.

Acknowledgments

Funding for CIPS data evaluation, and for the AIM mission, was provided by the NASA Small Explorer program. The SBUV/2 data were obtained from NOAA/NESDIS with support from the NOAA Climate and Global Change Atmospheric Chemistry Element. Some of this work was supported by Grant NNX06AC96G from NASA's Office of Space Science.

References

Bailey, S.M., Merkel, A.W., Thomas, G.E., Carstens, J.N., 2005. Observations of polar mesospheric clouds by the student nitric oxide explorer. Journal of Geophysical Research 110, D13203, doi:10.1029/2004JD005422.

Bailey, S.M., Thomas, G.E., Rusch, D.W., Merkel, A.W., Jeppesen, C.D., Carstens, J.N., Randall, C.E., McClintock, W.E., Russell III, J.M., 2008. Phase functions of polar mesospheric cloud ice as observed by the CIPS instrument on the AIM satellite. Journal of Atmospheric and Solar-Terrestrial Physics, this issue.

Chandran, A., Rusch, D.W., Palo, S.E., Thomas, G.E., Taylor, M.J., 2008. Gravity wave observation from the Cloud Imaging and Particle Size (CIPS) experiment on the AIM spacecraft. Journal of Atmospheric and Solar-Terrestrial Physics, this issue.

DeLand, M.T., Shettle, E.P., Thomas, G.E., Olivero, J.J., 2003. Solar backscattered ultraviolet (SBUV) observations of polar mesospheric clouds (PMCs) over two solar cycles. Journal of Geophysical Research 108(D8), 8445, doi:10.1029/2002JD002398.

DeLand, M.T., Shettle, E.P., Thomas, G.E., Olivero, J.J., 2006. A quarter-century of satellite polar mesospheric cloud observations. Journal of Atmospheric and Solar-Terrestrial Physics 68, 9–29.

DeLand, M.T., Shettle, E.P., Thomas, G.E., Olivero, J.J., 2007. Latitude-dependent long-term variations in polar mesospheric clouds from SBUV version 3 PMC data. Journal of Geophysical Research 112, D10315, doi:10.1029/2006JD007857.

Fleig, A., McPeters, R., Bhartia, P., Schlesinger, B., Cebula, R., Klenk, K., Taylor, S., Heath, D., 1990. Nimbus 7 Solar Backscatter Ultraviolet (SBUV) Ozone Products User's Guide. NASA.

Frederick, J.E., Cebula, R.P., Heath, D.F., 1986. Instrument characterization for the detection of long-term changes in stratospheric ozone: an analysis of the SBUV/2 radiometer. Journal of Atmospheric and Oceanic Technology 3, 472–480.

Heath, D.F., Krueger, A.J., Roeder, H.A., Henderson, B.D., 1975. The solar backscatter ultraviolet and total ozone mapping spectrometer (SBUV/TOMS) for Nimbus G. Optical Engineering 14, 323–331.

McClintock, W.E., Rusch, D.W., Thomas, G.E., Merkel, A.W., Lankton, M.R., Drake, V.A., Bailey, S.M., Russell III, J.M., 2008. The Cloud Imaging and Particle Size (CIPS) experiment on the Aeronomy of Ice in the Mesosphere (AIM) spacecraft. Journal of Atmospheric and Solar-Terrestrial Physics, this issue.

McPeters, R.D., Miles, T., Flynn, L.E., Wellemeyer, C.G., Zawodny, J.M., 1994. Comparison of SBUV and SAGE II ozone profiles: implications for ozone trends. Journal of Geophysical Research 99, 20513.

Merkel, A.W., Rusch, D.W., Palo, S.E., Russell III, J.M., Bailey, S.M., 2008. Planetary wave activity in polar mesospheric clouds as observed from the cloud imaging and particle size instrument. Journal of Atmospheric and Solar-Terrestrial Physics, this issue.

Rusch, D.W., Thomas, G.E., McClintock, W.E., Merkel, A.W., Bailey, S.M., Russell III, J.M., Randall, C.E., Jepessen, C.D., Callan, M., 2008. The cloud imaging and particle size experiment on the Aeronomy of Ice in the Mesosphere mission: cloud morphology for the northern 2007 season. Journal of Atmospheric and Solar-Terrestrial Physics, this issue.

Russell III, J.M., Mlynczak, M.G., Gordley, L.L., Larry, Tansock, J.J., Esplin, R., 1999. An overview of the SABER experiment and preliminary calibration results. Proceedings of SPIE 3756, 277–288.

Russell III, J.M., Bailey, S.M., Gordley, L.L., Rusch, D.W., Horanyi, M., Hervig, M.E., Thomas, G.E., Randall, C.E., Siskind, D.E., Stevens, M.H., Summers, M.E., Taylor, M.I., Englert, C.R., Espy, P.J., McClintock, W.E., Merkel, A.W., 2008. The Aeronomy of Ice in the Mesosphere (AIM) mission: overview and early science results. Journal of Atmospheric and Solar-Terrestrial Physics, this issue, doi:10.1016/j.jastp.2008.08.011.

Taylor, M.J., Gadsden, M., Lowe, R.P., Zalcik, M.S., Brausch, J., 2002. Mesospheric cloud observations at unusually low latitudes. Journal of Atmospheric and Solar-Terrestrial Physics 64, 991–999.

Thomas, G.E., 1996a. Is the polar mesosphere the miner's canary of global change? Advances in Space Research 18, 149–158.

Thomas, G.E., 1996b. Global change in the mesosphere–lower thermosphere region: has it already arrived? Journal of Atmospheric and Solar-Terrestrial Physics 58, 1629–1656.

Thomas, G.E., Olivero, J.J., Jensen, E.J., Schroeder, W., Toon, O.W., 1989. Relation between increasing methane and the presence of ice clouds at the mesopause. Nature 338, 490–492.

Thomas, G.E., McPeters, R.D., Jensen, E.J., 1991. Satellite observations of polar mesospheric clouds by the solar backscattered ultraviolet radiometer: evidence of a solar cycle dependence. Journal of Geophysical Research 96, 927–939.